Estimation to the turbulent kinetic energy dissipation rate and bottom shear stress in the tidal bottom boundary layer of the Yellow Sea*

LIU Zhiyu** and WEI Hao

(Key Laboratory of Physical Oceanography, State Education Ministry, Ocean University of China, Qingdao 266003, China)

Accepted on October 17, 2006

Abstract High frequency velocity fluctuations were measured by using an acoustic Doppler velocimeter (ADV) in the tidal bottom boundary layer (BBL) of the Yellow Sea (YS) for 25 h. The turbulent kinetic energy dissipation rate and the bottom shear stress were estimated and analyzed. Results show that: (1) in the tidal BBL of the YS, the variations of the dissipation rate and the bottom shear stress during 25 h are $(1.8\times10^{-8}$—$3.4\times10^{-5})$ $W\cdot kg^{-1}$ and $(6.6\times10^{-4}$—$7.5\times10^{-1})$ $N\cdot m^{-2}$ respectively, indicating that there are strong dissipations in the tidal BBL of the YS; (2) in the well-mixed tidal BBL, the turbulence is mainly shear-induced locally and the production and dissipation are generally in equilibrium; (3) for the seas where the semidiurnal tidal current is dominant, both the dissipation rate and the bottom shear stress exhibit a strong quarter-diurnal variation; (4) the mean bottom drag coefficient $\bar{C}_d(0.45)$ is 0.0017 (corresponding $\bar{C}_d(1.00)=0.0015$), but it has significant variations (0.0005—0.0082). The mean bottom roughness length is 2.8×10^{-5} m.

Keywords: ***tidal bottom boundary layer, turbulent kinetic energy dissipation rate, bottom shear stress, ADV, the Yellow Sea.***

In the coastal water, the momentum and energy balance are influenced by several parameters, among which the bottom shear stress and the turbulent kinetic energy dissipation rate are of particular significance[1]. The bottom shear stress affects circulation and controls the erosion, resuspension, deposition and flocculation of sediments[2]. The turbulent kinetic energy dissipation rate is a controlling factor for the entire turbulent energy budget. Thus, the understanding and modeling of coastal circulation, sediment transport, pollutant dispersal and biological processes rely on the knowledge of the turbulence characteristics in the bottom boundary layer (BBL)[1].

As a typical shallow sea with a mean depth of 44 m, the Yellow Sea (YS) is one of the principal regions of global ocean with strong tidal dissipation. With satellite altimeter data from TOPEX/POSEIDON, Ref. [3] shows that the tidal dissipation of the principal lunar semi-diurnal tide M_2 in the YS is about 150 GW. Numerical modeling studies indicated that there is intense tidal mixing in the YS, and the eddy viscosity can be as high as 10^{-3}—10^{-2} $m^2\cdot s^{-1}$[4,5]. Although there are already some investigations on the tidal dissipation and turbulent mixing in the YS[3—5], all of which are based on numerical modeling or satellite data, there are still no direct observations of the tidal dissipation and turbulent mixing. Most of the previous investigations are based on the "box model", in which it is assumed that the barotropic tide energy is totally dissipated in the turbulent BBL. The "box model" of tidal dissipation, which is also called "BBL method", was firstly proposed by Taylor[6] in his classic paper on tidal dissipation in the Irish Sea, and was then followed by Jefferys[7] in his estimates of global tidal dissipation. The "box model" has been used extensively in many tide models. According to the "box model", the tidal dissipation is proportional to the cube of the tidal currents. Thus, the BBL of the shallow sea will dissipate more than 99% of the global tidal energy, since typical tidal currents are of the order of 1 $cm\cdot s^{-1}$ in the deep seas, while of the order of 50 $cm\cdot s^{-1}$ in coastal waters[8]. However, Ref. [3] shows that approximately 25%—30% of the total tidal energy dissipation occurs in the deep ocean, generally near areas of rough topography. This is because the barotropic tide energy is not dissipated by the bottom friction only: on one hand, barotropic tidal currents can generate turbulence via the bottom shear stress, and then induce turbulent mixing and energy dissipation through the water column; on the other hand, internal tides can be generated by tide-topography interactions in the stratified seas. The energy of the internal tides is transferred to smaller and smaller scales through nonlinear wave-wave interac-

* Supported by the National Program on Key Basic Research Projects (Grant No. 2006CB400602)

** To whom correspondence should be addressed. E-mail: zhiyuliu@ouc.edu.cn

tions, and then induces turbulent mixing and energy dissipation. Therefore, it is necessary to conduct the direct observations of dissipation rate and turbulent mixing characteristics in the BBL.

To study the dynamics in BBL, vertical structures of shear stress and turbulent kinetic energy production, the turbulent mixing characteristics and its temporary and spatial variations in early winter in the YS, we conduced a 25 h continuous observation on a bottom-mounted platform at station A3 (36.04°N, 120.32°E) near the mouth of the Jiaozhou Bay in December 2005. In this contribution, we present the estimates of the turbulent kinetic energy dissipation rate and the bottom shear stress from the acoustic Doppler velocimeter (ADV) measurements in the BBL.

1 Observations and data processing

1.1 Instruments configurations in the observations

The observations of turbulence characteristics in the BBL and the water interior in early winter were carried out at a bottom-mounted station A3 (36.04°N, 120.32°E) (Fig. 1) near the mouth of the Jiaozhou Bay, Chinese coast of the YS in December 2005. The measurements of current profiles, high frequency velocity fluctuations near the sea floor and the Conductivity-Temperature-Depth (CTD) profiles from 15:00 Dec.14 to 16:00 Dec.15 2005 were taken on board of R/V Dongfanghong-2. During the 25 h measurements, the mean water depth was 18.1 m and the tidal range was 3.3 m.

A 6 MHz Nortek "Vector" ADV, a 600 kHz RDI ADCP, a Nortek 2 MHz Aquadopp Profiler (ADP), three RBR XR-420 CTDs and an optical backscatter system (OBS) were mounted on a frame on the seabed. The "upward looking" acoustic Doppler current profiler (ADCP) at a height of 1.0 m above the seabed was set up to record the along-beam velocities with a ping rate of 2 Hz continuously. The bin size was set to 0.75 m and the data were ensemble averaged over 2 s (i.e. four pings) before recorded. The ADV, at a height of 0.45 m above the bed (mab), was set up to sample continuously with a sampling frequency of 16 Hz. The "downward looking" ADP at a height of 0.85 mab was set up to work continuously with a sampling internal of 6 s and 0.25 m bin size. The CTD recorders on the frame were used to record temperature, salinity (conductivity)

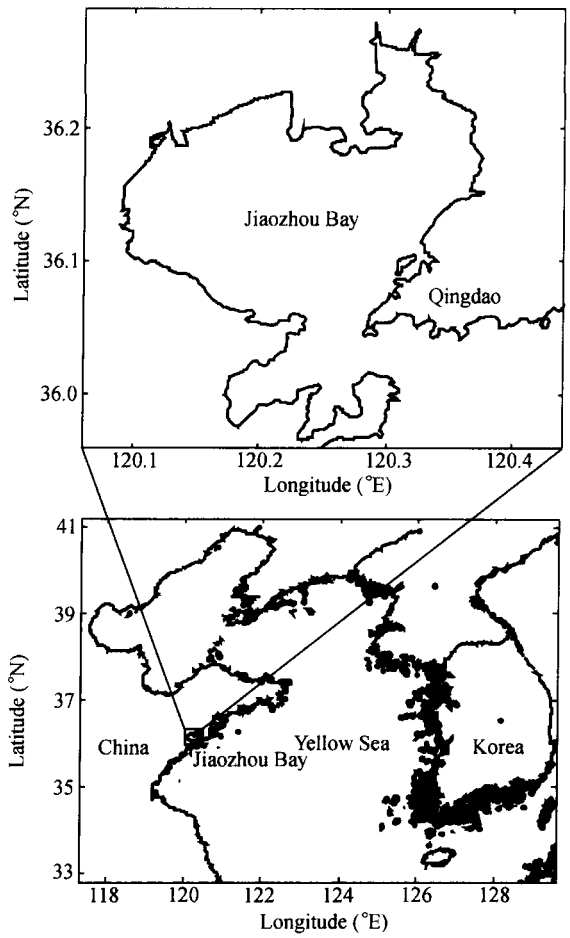

Fig. 1. Observation station A3.

and depth (pressure) every 5 s at three different heights (0.5 mab, 1.0 mab and 1.5 mab). The OBS was used to record sediment concentrations at a height of 0.85 mab, and was programmed for 15 s burst sampling every 5 min. During the 25 h measurements, a series of CTD casts were carried out near the bottom-mounted frame every 30 min with an RBR XR-620 CTD. The meteorological data were obtained every half an hour by using the onboard Auto-Meteorological-Station.

The ADV is a new type of acoustic Doppler current meter, which has a much smaller sampling volume compared with electromagnetic current meters (EMCMs) or ADCP. ADV extends frequency response, since the maximum useful sampling rate is inversely proportional to sensor dimension[8]. It has been successfully applied in a number of recent observational campaigns designed to validate its utility and improve our understanding of the interaction between turbulence, stratification, and shear in coastal waters[9—11]. The 6 MHz Nortek "Vector" ADV used

in the present study has a sampling volume of 883—3533 mm^3 (a cylinder, 5—20 mm in length and 15 mm in diameter, with a distance of 0.15 m from the sensor head). Its maximum internal sampling frequency and output frequency are 250 Hz and 64 Hz respectively, and it has an accuracy of 0.5% of the measured value ± 0.1 $cm \cdot s^{-1}$. As mentioned above, the ADV was set up to sample continuously with a sampling frequency of 16 Hz. Thus 25 h turbulent data with 16 Hz sampling frequency were obtained.

1.2 Meteorological conditions and background hydrography

The wind forcing was relatively stable during the whole 25 h period of the measurements with the mean speed of northwestern wind $\langle W_a \rangle = 9.3$ $m \cdot s^{-1}$ and the rms $(W_a) = 1.7$ $m \cdot s^{-1}$. The wind direction maintained between 290° and 330°. Owing to the fact that the distance between the observation station A3 and the shore is only 1.2 km the wind was of northwest direction, and the wind area was very small. The sea surface was calm and no obvious swell was observed. The pressure data, obtained by the XR-420 CTD on the bottom-mounted frame, indicated that the sea surface wave height was about 0.20 m. During the observation the heat forcing at the sea surface is mainly the differences between sea and atmosphere temperature. In the 25 h measurements the atmosphere temperature at the sea surface varied from -4 to 0 ℃ while the sea surface temperature (SST) varied from 7.0 to 8.5 ℃. The mean air-sea temperature difference $\langle T_w - T_a \rangle$ was 10.1℃.

By using the bulk formula of the sea surface wind stress and the heat flux, the momentum flux and the buoyancy flux can be calculated from the wind speed, relative humidity, air temperature and the SST. In the present study, the Matlab Air-Sea Interaction Toolbox was used (http://sea-mat.whoi.edu). The results showed that the mean surface friction velocity $\langle u_* \rangle$ was 1.1×10^{-2} $m \cdot s^{-1}$ during the measurements. This is a characteristic u_* for a mild storm, which produced the energy flux of 1.37 $W \cdot m^{-2}$ on the average. The average buoyancy flux at the sea surface was -1.3×10^{-7} $W \cdot kg^{-1}$. This value, as will be shown later, is comparable with the dissipation of turbulent kinetic energy generated by tidal current in the BBL. The negative buoyancy flux ensures strong convection at the sea surface and the upper layer.

The temperature-salinity profiles obtained by the XR-620 CTD Profiler (every 30 min) indicated that the water above the bottom layer was well mixed. The temperature was mainly isothermal across the whole water column. The temperature ranged from 7.1 to 8.1℃ with time during the observations. The water density was not as homogeneous vertically as the temperature due to the small differences of the salinity between different water layers. But the Brunt-Väisälä frequency N was very small and the maximum value during the observations was only 2.8×10^{-3} Hz. The data obtained by the XR-420 CTD on the bottom-mounted frame indicated that, the near-bottom temperature varied irregularly in time in the same range of 7.1—8.1℃ as the temperature of upper column. Furthermore, measurements of ADCP and ADP gave the velocity structures through the whole water column, showing that apart from the tidal BBL and the sea surface boundary layer where the current velocity increased with the distance from the boundary, the differences between the current velocities of different depths were very small. The flow was barotropic. In this study, our main focus has been on the analyses of the turbulent characteristics of the BBL based on the turbulent data obtained by ADV, therefore, no more detailed descriptions of the measurements from other instruments will be presented.

1.3 ADV data processing

The original ADV data were the 3 velocity components in the sampling volume in the earth coordinates (u, v, w), where u, v, w are the eastward, northward and vertical (positive upward) velocity components, respectively. We first divided the original data into groups by every 5 min. Thus, the 25 hours' data were divided into 300 groups. For the study on the inter-tidal variations of the turbulent characteristics the 5 min (the phase of the M_2 component changes by 2.4°) time interval is short enough. The preliminary analyses of the data indicated that taking the Reynolds averaged time interval as 1 min is proper. The analyses of the data of the first minute of each group were conduced. Firstly, every time series of 1 min was processed as follows:

(i) Filtering the time series of the 3 velocity components to remove the variations of low frequency and calculating the averaged current speed and direction;

(ii) taking the X axis in the direction of the averaged velocity, and calculating the fluctuations of the velocity components in the new coordinates u', v' and w';

(iii) removing the noises from the time series of the fluctuations of the velocity. In this study the "Phase-space thresholding method" proposed by Goring et al.[12] was used.

1.4 Estimates of turbulent kinetic energy dissipation rate

Estimating turbulent kinetic energy dissipation rate from high frequency velocity fluctuations is based on fitting measured fluctuation spectra to their respective theoretical and universal forms, within the inertial subrange of the wavenumber spectrum, and it is called inertial dissipation method[2,13—15]. The inertial subrange is an intermediate range of turbulent scales or wavelengths that is smaller than the energy-containing eddies, but larger than viscous eddies, in which the net energy coming from the energy-containing eddies is in equilibrium with the net energy cascading to smaller eddies where it is dissipated.

When a turbulent BBL is well-developed, a local balance holds between the energy input from large scale eddies and the small-scale dissipation, which leads to a one-dimensional spectrum of the form

$$\phi_{ii}(k) = \alpha_i \varepsilon^{2/3} k^{-5/3}, \quad (1)$$

where $\phi_{ii}(k)$ is the power spectral density of i-th velocity component ($i = 1, 2, 3$) at the wavenumber k. The constant α_i is the one dimensional Komolgorov universal constant, and has been experimentally determined, when the axis 1 is in the direction of the mean flow, $\alpha_1 = 0.53$, $\alpha_2 = \alpha_3 = \frac{4}{3}\alpha_1 \approx 0.71$[16].

Since the velocity data were obtained in a time domain we need transfer frequency spectra to wavenumber spectra. When $k\phi_{ii}(k)/U^2 \ll 1$, Taylor's "frozen turbulence" hypothesis can be applied. Assuming

$$k = \frac{2\pi f}{U}, \quad (2)$$

$$k\phi_{ii}(k) = f\phi_{ii}(f), \quad (3)$$

where f is frequency, and U the advection velocity, i.e. the mean velocity. As mentioned above, there are two requirements for the application of the inertial dissipation method: (i) the turbulence is well-developed, i.e. $Re = u_* \kappa z/\upsilon > R_c$, where u_* is the friction velocity, $\kappa = 0.40$ is von Kámán constant, υ the kinetic viscosity, and $R_c \approx 3000$[17] the critical Reynolds number; (ii) the velocity fluctuations are much less than the mean velocity. All the data used in this study satisfy the two requirements, so the dissipation rate can be estimated with the inertial dissipation method. Near the bed, vertical velocities are less contaminated by waves than horizontal velocities are, and the fluctuations w' are more likely to be due to the turbulence[18]. Thus, in this study, we systematically applied the inertial dissipation method only to estimate the turbulent energy dissipation rates based on the vertical velocities.

The inertial dissipation subrange was sought by visual inspection of the plots of the power spectrum density and fixed to be between 0.3 Hz and 2 Hz. Therefore, the dissipation rates were estimated by

$$\varepsilon_{spec} = 2\pi U^{-1} \alpha_i^{-3/2} [f^{5/2} \phi_{ii}^{3/2}(f)], \quad (4)$$

where the square brackets means averaged in the inertial subrange.

1.5 Estimates of bottom shear stress

In the BBL, the bottom shear stress can be estimated with three methods: the eddy correlation method, velocity profile method and dissipation method. The first method utilizes direct measurements of the high frequency turbulent fluctuations in the logarithmic layer, the second method utilizes the observations of mean velocity profiles in the logarithmic layer, and the third one is based on the observations or estimates of the turbulent kinetic energy dissipation rate in the constant stress layer (CSL). It is worthy to keep in mind that all the three methods have the same potential requirement that the sensor should be located in the CSL. Since the data are the high frequency turbulent fluctuations at a fixed location, we will utilize the eddy correlation method to estimate the bottom shear stress.

For a tidal BBL, the ratio of inertial force to friction can be scaled by $\omega z^2/A_z$, where ω is the tidal radian frequency, A_z the viscosity and z the elevation above the sea bed. For the YS, where the tide is predominantly semidiurnal M_2, $\omega \approx 1.4 \times 10^{-4}$ s^{-1}. In the weak-stratified shallow waters, a conservatively low estimate of A_z is 10^{-3} $m^2 \cdot s^{-1}$[19]. Thus, from $\omega z^2/A_z \leqslant 10^{-1}$ (i.e. inertial force is much less than friction), we obtain $z \leqslant \sqrt{0.1 A_z/\omega} \approx 0.85$ m, and it is the low estimate of the height of the tidal BBL. The sampling volume of ADV was at a

height of 0.45 mab in our observation, and it was in the CSL, so the bottom shear stress can be estimated with the eddy correlation method, i.e.

$$\tau_b = \rho(-\overline{u'w'}, -\overline{v'w'}), \quad (5)$$

where ρ is the seawater density, and u', v' and w' are the turbulent fluctuations of the three velocity components, respectively. And the friction velocity is given by

$$u_* = \sqrt{\frac{|\tau_b|}{\rho}} = [\sqrt{(-\overline{u'w'})^2 + (-\overline{v'w'})^2}]^{\frac{1}{2}}. \quad (6)$$

1.6 Logarithmic layer and law-of-the-wall

In the BBL, the mean velocity distribution is a function of the bottom shear stress τ_0, the bottom roughness length z_0, the distance to the bottom z, the seawater density ρ and the dynamic viscosity μ. The characteristic velocity scale in the BBL is called the friction velocity, $u_* = \sqrt{\tau_0/\rho}$. The Reynolds stress in the BBL is constant, and is equal to the bottom shear stress τ_0.

According to Prandtl mixing length theory, mixing length $l = \kappa z$, so the mean shear in the BBL is given by

$$\frac{\partial U}{\partial z} = \frac{u_*}{\kappa z}, \quad (7)$$

where U is the mean velocity, and $\kappa = 0.40$ is von Kármán constant. Integrating Eq. (7), we obtain

$$U(z) = \frac{u_*}{\kappa}\ln(z/z_0), \quad (8)$$

where z_0 is an integration constant and represents a length scale proportional to the roughness elements at the bottom. z_0 is customarily called bottom roughness length. Eq. (8) is the logarithmic velocity profile in the BBL, and the BBL is thus also called logarithmic layer.

In the well-mixed turbulent boundary layer, there is a local balance between the rate of production of the turbulent kinetic energy through the Reynolds stress working on the mean shear and the rate of the viscous dissipation of that energy, that is

$$-\overline{u'w'}\frac{\partial U}{\partial z} = \varepsilon, \quad (9)$$

where ε is the dissipation rate of turbulent kinetic energy per unit mass. In the logarithmic layer, the Reynolds stress is equal to the bottom shear stress, that is $-\overline{u'w'} = \tau_0$, along with the mean shear given by Eq. (7) and the definition of the friction velocity, it can be obtained that

$$\frac{u_*^3}{\kappa z} = \varepsilon. \quad (10)$$

This is the classical law-of-the-wall.

2 Results and discussion

In Fig. 2 the near-bottom mean velocity magnitude and direction, and the eastward and northward components of the velocity measured by the ADV are shown. During the 25 h period of the measurements, the near-bottom velocity magnitude varied from 0.01 to 0.50 $m \cdot s^{-1}$. The northward component (v) was much smaller than the eastward component (u) in the whole period. Therefore, the mean velocity was basically east-westward. This shows that the tidal current here is rectilinear (east-west). The eastward component of the current velocity exhibited obvious M_2 feature, while the northward component didnot show obvious tidal signal. Because the location is near the shore and the shore is basically along the east-west direction, we suggest that the northward component should have been induced by the interactions between the east-westward tidal current, the boundary and the topography, but not only by tidal component. Numerical modeling results showed that, the tidal waves at the open sea outside the Jiaozhou Bay were propagated from the northeast to the southwest. It is an anticlockwise tidal wave system. The flooding tidal water flows into the bay through the northeast part of the bay mouth. While, the ebb water flows to northeast part of the bay mouth along with the tidal inflow though the southeast part of the bay mouth[20]. For station A3 at the northeastern side of the bay mouth, the flooding tidal current is mainly the M_2 tidal current from the YS. Therefore, the near-bottom mean velocity is mainly the M_2 tidal current. During the ebb, the current from the bay meets the ebb current from the southwest of the bay mouth and they interact with each other, leading to the irregular variations of the near-bottom mean velocity at station A3 during the ebb. Apart from the M_2 tidal current there are some relatively high frequency currents.

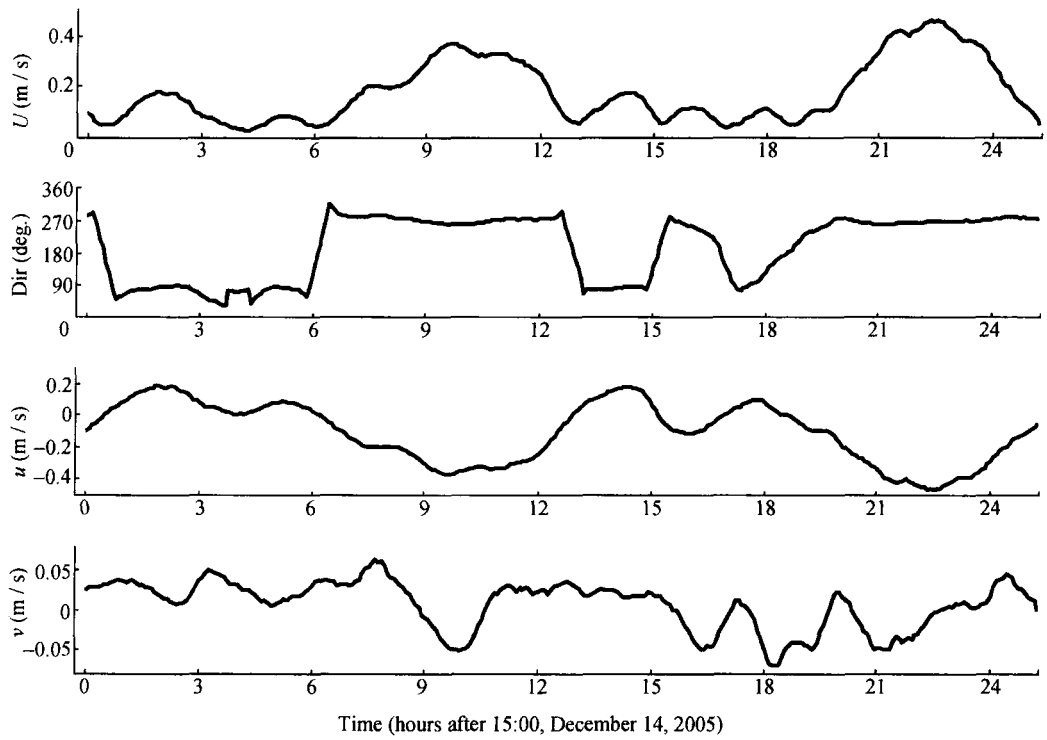

Fig. 2. Time series of the near-bottom mean velocity magnitude, direction, the eastward component and the northward component.

The ε_{spec}-u_* dependence and the classical law-of-the-wall for $z = 0.45$ m are shown in Fig. 3. It can be seen that ε_{spec} and u_* have a pretty good correlation in term of the classical law-of-the-wall. This indicates that, in the BBL of the coastal waters, the turbulence is generally shear-induced locally and the production and dissipation are generally in equilibrium. The velocity distribution with the height from the seabed is logarithmic.

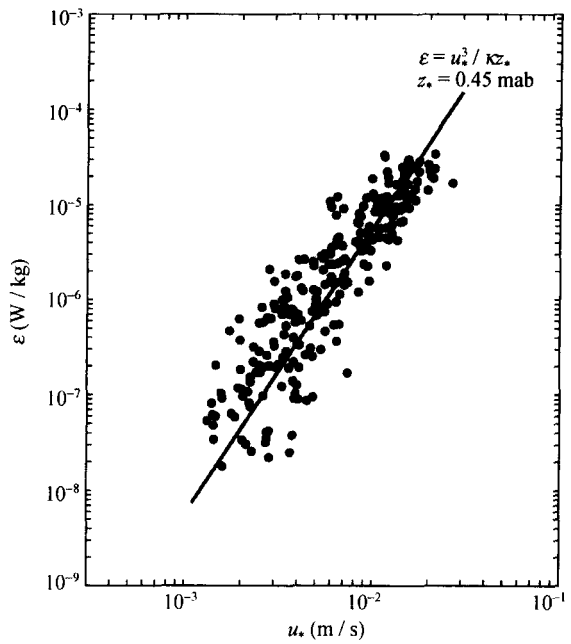

Fig. 3. The ε_{spec}-u_* dependence compared with the law-of-the-wall for $z = 0.45$ mab.

Fig. 4 shows the time variations of near-bottom mean velocity magnitude U (black dot-dash line), friction velocity u_* (red dashed line), and the dissipation rate ε_{spec} (blue solid line). Both the friction velocity and dissipation rate almost exactly follow the near bottom velocity magnitude, indicating that turbulence here was mainly shear-induced locally. For the seas where the semi-diurnal tidal current is dominant, both the dissipation rate and the bottom shear stress exhibit a strong quarter-diurnal variation.

The bottom drag coefficient $C_d(z)$ can be obtained based on the friction velocity u_* and the mean velocity magnitude $U(z)$ at a given height z:

$$C_d(z) = u_*^2 / U(z)^2. \quad (11)$$

The sampling volume of the ADV is 0.45 m above the seabed, therefore the drag coefficient $C_d(0.45)$ can be calculated from the friction velocity and the near-bottom mean velocity magnitude. Results showed that, the mean value of $C_d(0.45)$ during the 25 h measurements, defined as $\overline{C}_d(0.45) = \exp\left\{\frac{1}{n}\sum_{i=1}^{n} \ln[C_{d_i}(0.45)]\right\}$ $(n = 300)$, was

0.0017. The corresponding mean value of $C_d(1.00)$ was 0.0015, consistent with the common knowledge about this region[21]. However, $C_d(0.45)$ varied obviously from 0.0005 to 0.0082 during the measurements.

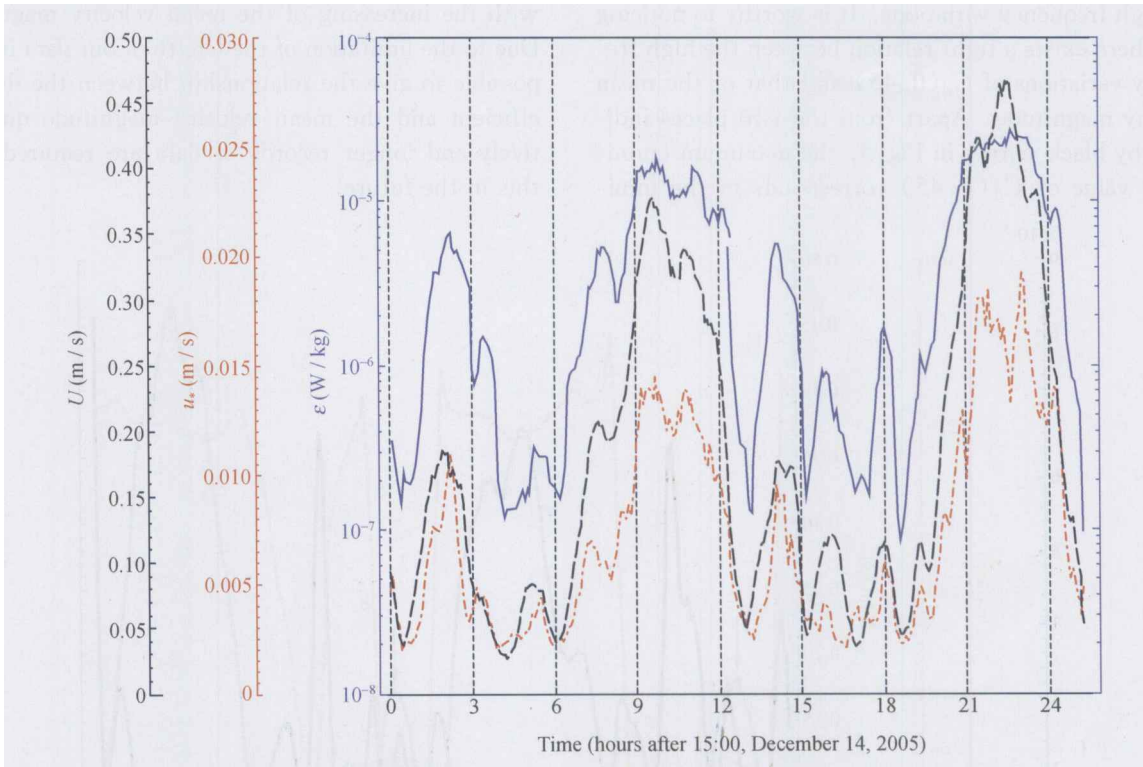

Fig. 4. Time series of near-bottom mean velocity magnitude (black dot dashed line), friction velocity (red dashed line) and dissipation rate (blue solid line).

As regard to the variation of the drag coefficient there are many possible affecting factors: the local topography caused form drag, the wave-current interaction, changes in the boundary layer flow regime, the stratification of the boundary layer by suspended sediments[22]. Using the ADCP data obtained in South San Francisco Bay, USA, Cheng et al.[23] analyzed the variations of the daily mean drag coefficient. Their results showed that the drag coefficient had a higher value during less energetic neap tides and had a lower value during more energetic spring tides. When the velocity was larger than a critical value (0.25—0.30 $m \cdot s^{-1}$ in their case) the logarithmic roughness length $\ln z_0$ decreased approximately linearly with increasing velocity. They hypothesized that this was because the critical velocity corresponds to the critical bottom shear stress of the sediment erosion. High free-stream velocity resulted in more effective erosion and a reduction in form drag at the sediment-water interface and hence smaller value of bottom roughness length. When the velocity was less than the critical value, the sediment deposition began to take place, and the deposited sediments created random irregularities at bed surface that led to higher value of roughness and drag coefficient. Howarth et al.[24] based on the observed data of the bottom stress at seven stations in the North Sea obtained that the mean drag coefficient is proportional to the amplitude of the M_2 tidal component: $C_d = 0.001 \times [0.59 + 0.78 \times M_2]$, where M_2 represents the amplitude of the M_2 tidal component. Refs. [23, 24] involve the study of the inter-tide variations or the long term averaged values of the drag coefficient. As regard to the intra-tide variation of the drag coefficient there is yet no report. Compared with the inter-tide variation the intra-tide variation of the drag coefficient is more complicated.

Fig. 5 shows time variations of the drag coefficient $C_d(0.45)$ and the near-bottom mean velocity magnitude and direction. It can be seen that during the flood tide the mean velocity magnitude is comparatively large, and the direction is steady. The current is mainly the M_2 tidal current. $C_d(0.45)$ is comparatively small (less than the mean value of 0.0017 most of the time). It varies slightly from 0.001 to 0.002. During the ebb the velocity magnitude is comparative-

ly small, and there are obvious relatively high frequency variations. $C_d(0.45)$ varies conspicuously from 0.0005 to 0.0082 and at the same time there are high frequency variations. It is worthy to noticing that there exists a tight relation between the high frequency variations of $C_d(0.45)$ and that of the mean velocity magnitude. Apart from the two places indicated by black arrows in Fig. 5, the maximum (minimum) value of $C_d(0.45)$ corresponds to the minimum (maximum) value of the mean velocity magnitude. This indicates that the drag coefficient is dependent of the mean velocity magnitude and decreases with the increasing of the mean velocity magnitude. Due to the limitation of the length of our data it is impossible to give the relationship between the drag coefficient and the mean velocity magnitude quantitatively and longer records of data are required to do this in the future.

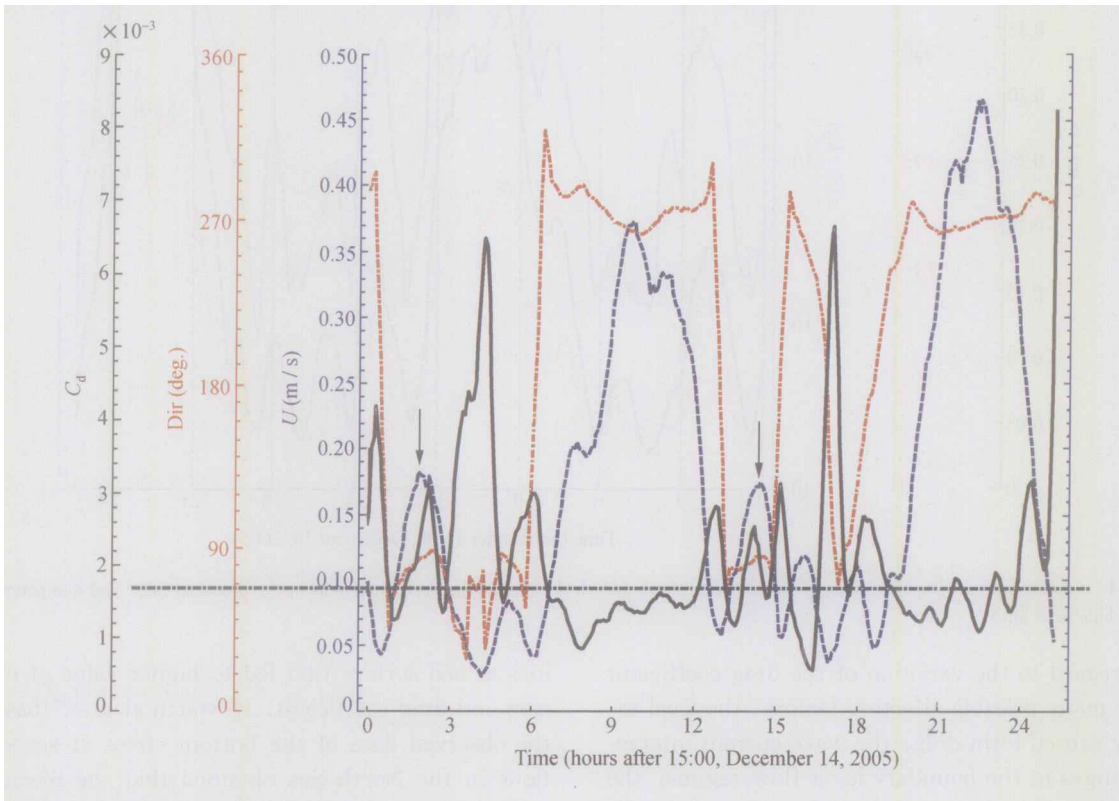

Fig. 5. Time series of the drag coefficient $C_d(0.45)$ (black solid line), the near-bottom mean velocity magnitude (blue dashed lined) and direction (red dot dashed line). The grey dot dashed line represents the mean value of $C_d(0.45)$, i.e. 0.0017.

In the logarithmic layer it can be obtained from (8) and (11) that

$$C_d(z) = \kappa^2 / [\ln(z/z_0)]^2. \quad (12)$$

Taking $C_d(45) = 0.0017$ and $z = 0.45$ m into the above equation, the mean bottom roughness length during the measurements can be obtained:

$$\bar{z}_0 = z / \exp(\kappa / \sqrt{\bar{C}_d})$$
$$= 0.45 / \exp(0.40 / \sqrt{0.0017})$$
$$= 2.8 \times 10^{-5} \text{ m}.$$

And this is consistent with the fact that the sea bed is muddy[25].

3 Conclusions

From the calculations and analyses of the 25 h turbulent data, we obtain the following conclusions:

(1) In the tidal BBL of the YS, the variations of the turbulent kinetic energy dissipation rate and the bottom shear stress during 25 h are (1.8×10^{-8}—3.4×10^{-5}) $W \cdot kg^{-1}$ and (6.6×10^{-4}—7.5×10^{-1}) $N \cdot m^{-2}$, respectively. This indicates that there are strong dissipations in the tidal BBL of the YS.

(2) In the well-mixed tidal BBL, the turbulence is generally shear-induced locally and the production and dissipation are generally in equilibrium.

(3) For the seas where the semi-diurnal tidal current is dominant, both the dissipation rate and the bottom shear stress exhibit a strong quarter diurnal

variation.

(4) The mean bottom drag coefficient $\bar{C}_d(0.45)$ is 0.0017 (corresponding $\bar{C}_d(1.0)=0.0015$), but it has significant variations (0.0005—0.0082). The mean bottom roughness length is 2.8×10^{-5} m.

References

1 Doron P. K., Bertuccioli L., Katz J. et al. Turbulence characteristic and dissipation estimates in the coastal ocean bottom boundary layer from PIV data. J. Phys. Oceanogr., 2001, 31(8): 2108—2134.

2 Kim S. C., Friedrichs C. T., Maa J. P. Y. et al. Estimating bottom stress in tidal boundary layer from acoustic Doppler velocimeter data. J. Hydr. Engrg., 2000, 126(6): 399—406.

3 Egbert G. D. and Ray R. D. Significant dissipation of tidal energy in the deep ocean inferred from satellite altimeter data. Nature, 2000, 405(15): 775—778.

4 Qiao F., Ma J., Xia C. et al. Influence of the surface wave-induced and tidal mixing on vertical temperature structure of the Yellow and East China Seas in summer. Progress in Natural Science, 2006, 16(7): 739—746.

5 Lee J. C. and Jung K. T. Application of eddy viscosity closure models for the M_2 tide and tidal currents in the Yellow Sea and East China Sea. Continental Shelf Research, 1999, 19(4): 445—475.

6 Taylor G. I. Tidal friction in the Irish Sea. Philosophical Transactions of the Royal Society of London (A), 1919, 220: 1—33.

7 Jeffreys H. Tidal friction in shallow seas. Philosophical Transactions of the Royal Society of London (A), 1921, 221: 239—264.

8 Munk W. H. Once again: once again—Tidal friction. Progress in Oceanography, 1997, 40: 7—35.

9 Soulsby R. L. Selecting record length and digitization rate for near-bed turbulence measurements. J. Phys. Oceanogr., 1980, 10 (2): 208—219.

10 Voulgaris G. and Trowbridge J. H. Evaluation of the acoustic Doppler velocimeter (ADV) for turbulence measurements. J. Atmos. Oceani. Technol., 1998, 15(1): 272—289.

11 Fugate D. C. and Chant R. J. Near-bottom shear stresses in a small, highly stratified estuary. J. Geophys. Res., 2005, 110: C3.

12 Goring D. G. and Nikora V. I. Despiking acoustic Doppler velocimeter data. J. Hydr. Engrg., 2002, 128(1): 117—126.

13 Gross T. F. and Nowell A. R. M. Spectral scaling in a tidal boundary layer. J. Phys. Oceanogr., 1985, 15(5): 496—508.

14 Dewey R. K. and Crawford G. B. Bottom stress estimates from vertical dissipation rate profiles on the continental shelf. J. Phys. Oceanogr., 1988, 18(8): 1167—1177.

15 Nimmo-Smith W. A. M., Katz J. and Osborn T. R. On the structure of turbulence in the bottom boundary layer of the coastal ocean. J. Phys. Oceanogr., 2005, 35(1): 72—93.

16 Sreenivasan K. R. On the universality of the Kolmogorov constant. Phys. Fluids, 1993, 7(11): 2778—2784.

17 Huntley D. A. A modified inertial dissipation method for estimating seabed stresses at low Reynolds numbers, with application to wave/current boundary layer measurements. J. Phys. Oceanogr., 1988, 18(2): 339—346.

18 Stapleton K. R. and Huntley D. A. Seabed stress determination using the inertial dissipation method and the turbulent kinetic energy method. Earth Surface Processes and Landforms, 1995, 20 (9): 807—815.

19 Friedrichs C. T. and Hamrick J. M. Effects of channel geometry on cross sectional variations in along channel velocity in partially stratified estuaries. Coastal and Estuarine Studies, 1996, 53: 283—300.

20 Editorial Board of Annals of Bays in China. Annals of Bays in China (Series 4) (in Chinese), Beijing: China Ocean Press, 1993, 448.

21 Guo X. and Yanagi T. Three-dimensional structure of tidal current in the East China Sea and the Yellow Sea. Journal of Oceanography, 1998, 54(6): 651—668.

22 Green M. O. and McCave I. N. Seabed drag coefficient under tidal currents in the eastern Irish Sea. J. Geophys. Res., 1995, 100(C8): 16057—16069.

23 Cheng R. T., Ling C. H. and Gartner J. W. Estimates of bottom roughness length and bottom shear stress in South San Francisco Bay, California. J. Geophys. Res., 1999, 104(C4): 7715—7728.

24 Howarth M. J. and Souza A. J. Reynolds stress observations in continental shelf seas. Deep-Sea Research II, 2005, 52(9—10): 1075—1086.

25 Soulsby R. L. The bottom boundary layer of shelf seas. In: Physical Oceanography of Coastal and Shelf Seas, 35, Elsevier Oceanography Series. Amsterdam: Elsevier, 1983, 189—266.